CMS Physics Analysis Summary

Contact: cms-pag-conveners-susy@cern.ch 2012/07/05

Search for physics beyond the standard model in events with τ-leptons in the presence of multijets and large momentum imbalance in pp collisions at $\sqrt{s} = 7$ TeV.

The CMS Collaboration

Abstract

A search for physics beyond the standard model is performed with one or more hadronically decaying τ-leptons, highly energetic jets and large momentum imbalance in the final state. The data sample corresponds to an integrated luminosity of 4.98 fb^{-1} of pp collisions at $\sqrt{s} = 7$ TeV collected with the CMS detector at the LHC. The number of observed events is consistent with predictions for standard model processes. In the absence of any evidence of suspersymmetry, upper limits on the mass of the gluino have been set.

1 Introduction

For the last few decades, the standard model (SM) of particle physics has been successful in explaining a wide variety of physics from microscopic to cosmological phenomena at collision energies up to the electroweak scale. In spite of this, the SM is incomplete as it possesses a divergence in the Higgs sector [1], fails to incorporate the gravitational force, and has no cold dark matter (DM) candidate [2–5]. Many models of physics beyond the SM have been proposed in order to address these problems.

DM particles, if produced in proton-proton collisions at the LHC, would escape detection and result in a significant momentum imbalance in the detector. Additionally, cascade decays of heavy colored particles in many physics beyond the SM (BSM) scenarios such as supersymmetry (SUSY) [2] would be accompanied by a high multiplicity of energetic jets in the final states. In certain models, the lightest supersymmetric particle (LSP) is a candidate for DM. It has been appreciated for some time that the DM relic density at freeze-out may be sensitive to coannihilation processes involving the LSP and the next-to-lightest supersymmetric particle (NLSP). Stau-neutralino coannihilation is characterized by a mass difference (ΔM) between the NLSP (stau) and the LSP (neutralino) of approximately 5-15 GeV. This narrow mass difference is necessary to allow the NLSP to coannihilate with the LSP in the early universe leading to the current dark matter density in the universe [6]. If the stau ($\tilde{\tau}$) becomes the NLSP and dominantly decays into a τ-lepton and an LSP, small values of ΔM will lead to final states with low energy τ-leptons ($p_{\mathrm{T}} \sim \Delta M$) from $\tilde{\tau}$ decays [7]. In the case of very small values of ΔM ($\sim$ 5 GeV), the low energy τ cannot be effectively detected and only the energetic τ from the decay of the neutralino can be observed. The search for SUSY with a single τ lepton has a better sensitivity in this case.

The $\tilde{\tau}$ is produced via charginos and neutralinos in cascade decays of colored SUSY particles. In about one third of cases, τ-leptons decay into lighter leptons plus neutrinos, whereas in about two thirds of the cases, τ-leptons decay into a hadronic system with one, three or five charged mesons that can be accompanied by neutral pions and a τ-neutrino. Hence, events with multi τ-leptons in the presence of a high multiplicity of jets is an interesting probe for new physics. Throughout this paper, the visible part of a hadronically decaying τ-lepton will be referred to as τ_h. In this paper we present a search for BSM particles in events with exactly one τ_h and jets, and with jets and two or more τ_h's. These two topologies have complimentary sensitivity to models with a wide range of values of ΔM.

The analysis is performed using data collected with the Compact Muon Solenoid (CMS) detector in proton-proton collisions at a center of mass energy of $\sqrt{s} = 7$ TeV at the Large Hadron Collider (LHC). The data samples correspond to an integrated luminosity of 4.98 ± 0.11 fb^{-1}. The search is characterized by data driven techniques developed to determine the backgrounds directly from data and to reduce the reliance on simulation.

To illustrate the sensitivity of this search for BSM processes, the constrained minimal supersymmetric extension of the standard model (cMSSM) or minimal supergravity (mSUGRA) models are chosen as benchmarks [2, 8, 9]. An interpretation of the results in the context of simplified models of supersymmetry (SMS) [10, 11] is also performed.

2 CMS Detector

The CMS experiment [12] uses a right-handed coordinate system, with the origin at the nominal interaction point, the x axis pointing to the center of the LHC ring, the y axis pointing up

(perpendicular to the LHC plane), and the z axis along the anticlockwise-beam direction. The polar angle, θ, is measured from the positive z axis and the azimuthal angle, ϕ, is measured in the x-y plane. The pseudorapidity is given by $\eta = -\ln\tan(\theta/2)$.

The central feature of the CMS apparatus is a superconducting solenoid, of 6 m inner diameter, providing a field of 3.8 T. Within the field volume are the silicon pixel and strip tracker, the crystal electromagnetic calorimeter (ECAL), which includes a silicon sensor preshower detector in front of the ECAL endcaps, and the brass/scintillator hadron calorimeter (HCAL). Muons are measured in gas-ionization detectors embedded in the steel return yoke. In addition to the barrel and endcap detectors, CMS has extensive forward calorimetry.

The inner tracker measures charged particles within $|\eta| < 2.5$ and provides an impact parameter resolution of ~ 15 μm and a transverse momentum (p_{T}) resolution of about 1.5 % for 100 GeV particles. Collision events were selected by a first level trigger made of a system of fast electronics and a higher level trigger that consists of a farm of commercial CPUs running a version of the offline reconstruction optimized for fast processing. A more detailed description of the CMS detector can be found elsewhere [12].

3 Object Reconstruction and Identification

The anti-k_T clustering algorithm [13] with $R = 0.5$ is used for jet clustering. The jets and transverse momentum imbalance in the detector ($\not\!\!E_{\mathrm{T}}$) are reconstructed with the Particle Flow (PF) algorithm [14]. Jets are required to pass jet identification criteria designed to reject anomalous behavior from the calorimeters and to be fairly well separated from any identified τ-leptons.

Aside from the main search, validation and efficiency studies are performed by utilizing $l + \tau_h$ in the final states, where $l = \mathrm{e}/\mu$. Muons are reconstructed using the tracker and muon chambers. Quality cuts based on the minimum number of hits in the silicon tracker, pixel detector and muon chambers are applied to suppress backgrounds from punch-throughs and decays in flight [15]. Electrons are reconstructed by combining tracks produced by the Gaussian Sum Filter algorithm with ECAL clusters. Requirements are imposed to distinguish prompt electrons from charged pions and from electrons produced by photon conversions [16]. The light lepton candidates are required to pass both track and ECAL isolation requirements. Track isolation is defined as the sum of the p_{T} of the tracks, as measured by the tracking system, within an isolation cone of radius $\Delta R = \sqrt{(\Delta\eta)^2 + (\Delta\phi)^2} = 0.4$ centered around the light lepton track. Similarly, ECAL isolation measures the amount of energy deposited in the ECAL within the isolation cone. In both cases the contribution from the light lepton candidate is removed from the sum.

Hadronic decays of the τ-lepton are reconstructed with the PF algorithm [17] which is used to form a mutually-exclusive collection of reconstructed particles (muons, electrons, photons, charged and neutral hadrons) by combining tracks and calorimeter clusters. Reconstruction and identification is performed using the hadrons plus strips (HPS) algorithm [18] designed to optimize the performance of τ_h reconstruction by considering specific τ_h decay modes. To suppress backgrounds in which light-quark or gluon jets can mimic hadronic taus, a τ_h is required to be spatially isolated from other energy in the event. Charged hadrons and photons not considered in the reconstruction of the τ_h decay mode are used to calculate isolation. Additionally, τ_h candidates are also required to be distinguishable from electrons and muons in the event. Two HPS isolation definitions are used in the analysis presented. The τ_h isolation definition used in the single τ_h final state rejects a τ_h candidate if one or more charged hadrons with $p_{\mathrm{T}} > 1.0$ GeV or one or more photons with transverse energy $E_{\mathrm{T}} > 1.5$ GeV are found within

the isolation cone of radius $\Delta R = 0.5$. The isolation definition used in the $\tau_h\tau_h$ final state requires no charged hadrons with $p_T > 1.5$ GeV and no photons with transverse energy $E_T > 2.0$ GeV within the isolation cone of radius $\Delta R = 0.3$. The isolation criteria used for the $\tau_h\tau_h$ final state increase the efficiency of selecting signal events while reducing the rate of misidentified events. This affects the event yield of the misidentified background events, which depends on the square of the misidentification rate. The total yield of misidentified events is thus much smaller in the $\tau_h\tau_h$ final state than in the single τ_h final state.

The missing transverse momentum $\not{H}_T$ is defined as

$$\not{H}_T = | - \sum \vec{p}_T^{\,jet} | \tag{1}$$

where the $\sum$ runs over all the jets in the event, with $p_T > 30$ GeV. The transverse hadronic momentum H_T present in the event is an estimator of the overall energy scale and is defined as $H_T = \sum p_T^{jet}$. For the single τ_h final state, H_T is calculated using jets with $p_T > 50$ GeV and will be referred to as H_T^{50}. For the $\tau_h\tau_h$ final state, H_T is calculated using jets with $p_T > 30$ GeV and will be referred to as H_T^{30}. In the $\tau_h\tau_h$ final state, the use of a lower cut on the p_T of the jets, increases the efficiency of signal events, without significantly increasing the efficiency of background events.

4 Signal and Background Samples

The major SM backgrounds are $t\bar{t}$ and W and Z production with associated jets where the jets are misidentified as τ_h. Both $t\bar{t}$ and W+jets events can have real τ_h's and large $\not{E}_T$ from W boson decays as well as jets that can be misidentified as τ_h. Neutrinos from the Z boson decay gives rise to large $\not{E}_T$ in $Z(\rightarrow \nu\bar{\nu})$ + jets and so these type of events become a background when one or more jets are misidentified as τ_h. $Z(\rightarrow \tau\bar{\tau})$ + jets becomes a background due to the presence of real τ-leptons in the event as well as large $\not{H}_T$ from the their decay into neutrinos. QCD multijet events can become a background when a badly mismeasured jet gives rise to large $\not{E}_T$ and jets are misidentified as τ_h.

Collision data is compared to samples of simulated events. Signal and background Monte Carlo (MC) samples are produced with the PYTHIA 6.4.22 [19] and MADGRAPH [20] generators using the Z2 tune and the CTEQ6.6 parton distribution function (PDF) set. The τ-lepton decays have been performed with TAUOLA [21]. MC generated events have been processed with a detailed simulation of the CMS apparatus using the GEANT4 package [22]. The MC yields are normalized to integrated luminosity using next-to-leading order (NLO) cross sections. At the LHC luminosity, the mean number of interactions in a single beam crossing that is used for this analysis, is approximately 8. In MC events, multiple interactions are superimposed on the hard collision, and the MC event is reweighted such that the distribution of reconstructed primary vertices matches that in data.

5 Event Selection

Events for both final states are selected using a trigger based on missing momentum ($\not{H}_T{}^{\text{online}} > 150$ GeV). This trigger was chosen in order to avoid imposing a high transverse momentum requirement on the τ_h candidate and in order to maintain sensitivity in regions where the p_T of the τ_h candidate is usually small ($p_T \sim 15$ GeV). This trigger is fully efficient for an offline cut of $\not{H}_T > 250$ GeV with an efficiency of $(98.9 \pm 2.5)\%$. For the τ_h efficiency and validation studies, samples are chosen using $\mu - \tau_h$ triggers.

The τ_h candidates must satisfy the kinematic selection of $p_T > 15$ GeV and $|\eta| < 2.1$ and must pass the τ_h identification criteria outlined in Section. 3. The single τ_h final state requires exactly one τ_h candidate and no additional light leptons (e,μ) in the event, in order to suppress W + jets, $t\bar{t}$, and Z + jets contributions. The $\tau_h\tau_h$ final state requires events to have ≥ 2 τ_h candidates with no additional light lepton veto on the event.

For the single τ_h final state, the baseline event selection used for testing background estimates requires $H_T^{50} > 350$ GeV and $\not{H}_T > 250$ GeV while the full selection defining the signal region (SR) requires $H_T^{50} > 600$ GeV and $\not{H}_T > 400$ GeV. The more stringent requirements for the full selection help to suppress background events since there are fewer handles to separate signal from background in events with only one τ_h.

For the $\tau_h\tau_h$ final state events with at least two jets with $p_T > 100$ GeV and $|\eta| < 3.0$ and $\not{H}_T > 250$ GeV are selected. Multijet events are rejected by requiring the difference in the azimuth ϕ between the $\not{H}_T$ and the next-to-leading jet to be $|\Delta\phi(j_2, \not{H}_T)| > 0.5$. Finally, events are required to contain at least one $\tau_h\tau_h$ pair well separated in η–ϕ space by $\Delta R(\tau_{h,i}, \tau_{h,j}) > 0.3$.

6 Background Estimate

The background contributions to the single τ_h final state are categorized differently from the $\tau_h\tau_h$ final state. In the single τ_h final state, the main background contributions are divided into events containing a real τ_h and events where a jet is misidentified as a τ_h. In the $\tau_h\tau_h$ final state, the main contribution comes from one or more jets being misidentified as a τ_h for different background sources and each background source is associated with a well defined control region (CR).

6.1 Estimate of Backgrounds in the Single τ_h Final State

In the single τ_h final state, the largest background contribution comes from W + jets events which contain a real τ_h while the other significant contribution comes from multijet events where the jet is misidentified as a τ_h. The real τ_h contribution is estimated using a sample of $W \to \mu\nu$ events, where the muon will have the same kinematics as the τ_h. The multijet background is estimated by applying the jet$\to \tau_h$ misidentification rate in a selected CR.

6.1.1 Estimate of the Real-τ_h Background in the Single τ_h Final State

The main background from SM processes in the single τ_h search region is the associated production of W + jets where the W decays into a τ_h. Assuming lepton universality, muons are produced in W-decays as often as τ-leptons. Therefore, $W(\to \mu\nu)$ + jets events where the muon is used to simulate a τ_h can be used as a control sample to estimate the background contribution from a real τ_h. Such a sample will be referred to as a muon control sample.

To select the muon control sample, events are required to contain no reconstructed τ_h or electron and to have exactly one muon. To emulate the τ_h acceptance, the muon is required to have a pseudorapidity of $|\eta| < 2.1$. The muons in the muon control sample are corrected for muon reconstruction efficiency (ε_μ) and muon isolation efficiency (ε_μ^{iso}). The muon reconstruction efficiency is derived from a sample of Z + jets events and parameterized as a function of p_T and η. The muon isolation criteria helps to distinguish between muons coming from the decay of the W boson and muons coming from multijet events. The isolation efficiency is parameterized as a function of the separation from the next jet and the relative momentum of the jet. A correction factor is applied to the muons in the muon control sample to account for the probability of the muon not coming from a τ-lepton decay (p_μ^W). This correction factor depends on the p_T of the

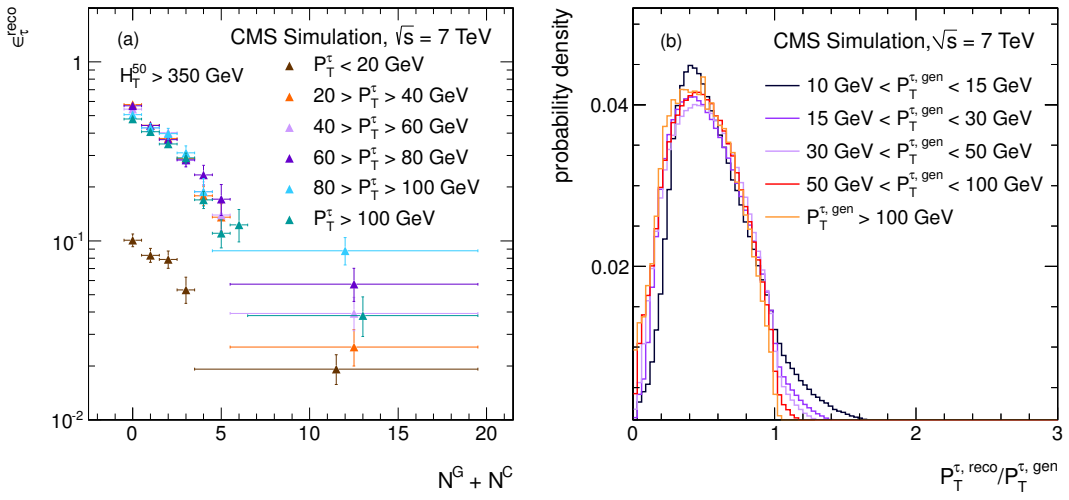

Figure 1: (a) Dependence of the τ_h reconstruction efficiency on the number of additional particles in the isolation cone in bins of τ_h p_T for the single τ_h final state where, N^G is the number of photons and N^C is the number of charged hadrons and (b) Dependence of $p_T^{\tau,gen}$ on the τ_h response. Both distributions are derived from a simulated sample of W + jets events.

muon and the amount of $\not{H}_T$ in the event and is derived from a simulated sample of W + jets events.

As the muons in the muon control sample are selected to mimic a τ_h a correction is applied for the probability (ε_τ) of reconstructing and identifying a τ_h. The reconstruction and identification efficiency is parameterized as a function of the p_T of the τ_h candidate and as a function of the number of additional particles in the isolation cone, which is the sum of the number of photons (N^G) and the number of charged hadrons (N^C) in the isolation cone (Fig. 1a). Corrections are also applied for the branching fractions of $W \to \mu\nu$ and $W \to \tau\nu$ ($f_\tau^{bf(hadr)}$). Except for the τ_h branching fraction, the values of the correction factors differ in each event. They are combined for an overall weight which is applied to each event and is defined as

$$f_{event}^{corr} = \frac{p_\mu^W \times \varepsilon_\tau \times f_\tau^{bf(hadr)}}{\varepsilon_\mu \times \varepsilon_\mu^{iso}} \tag{2}$$

A τ_h response template is derived from simulated events. The response template takes into account the ratio of the reconstructed energy of the τ_h to the true energy before the decay of the τ-lepton. The τ_h response depends on the transverse momentum of the generated τ-lepton (Fig. 1b) and on the number of reconstructed vertices in the event. The muon is smeared as a function of p_T and the number of vertices to mimic the p_T distribution of the visible τ_h.

Fig. 2 shows the H_T^{50} and $\not{H}_T$ distributions from simulated events of W + jets. These events pass the baseline selection described in Section 5. The reconstructed τ_h is required to match the visible part of the hadronically decaying generated τ-lepton. The event yield and distributions are compared to the prediction from the muon control sample and agree within statistical uncertainties and verify closure of the method in MC simulation. Hence, the predicted H_T^{50} and $\not{H}_T$ distributions from the muon control sample can be taken to describe a τ_h sample within statistical uncertainties.

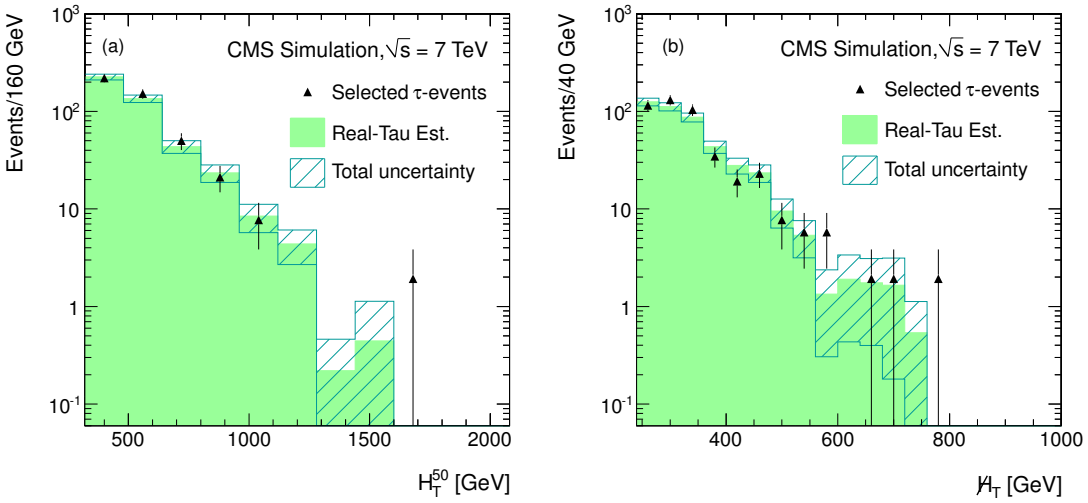

Figure 2: (a) Distributions of H_T^{50} and (b) $\not{H}_T$ for the real τ_h estimate in W + jets simulated events for the single τ_h final state. The black triangles are the simulated events that pass the baseline selection and have a reconstructed τ_h matched to the visible part of a generated, hadronically decaying τ-lepton. The filled green area is the prediction obtained from the muon control sample. The hashed area is the total uncertainty on the prediction.

Table 1: The estimated (predicted) and observed (selected) background contributions for simulated events with a real τ_h passing the baseline and full selection in the single τ_h final state. The reconstructed τ_h is required to match the visible part of the generated, hadronically decaying τ-lepton. The predictions are derived from the muon control sample and the events are normalized to 4.98 fb^{-1}.

L = 4.98 fb^{-1}	Baseline Selection		Full Selection	
	Selected	Predicted	Selected	Predicted
$Z(\to ll)$+ jets	10.9 ± 2.1	8.4 ± 1.3	0.8 ± 0.6	0.4 ± 0.3
W^+W^-	15.1 ± 1.6	14.4 ± 1.1	0.5 ± 0.3	1.3 ± 0.3
$t\bar{t}$	60.6 ± 3.7	63.2 ± 2.1	1.6 ± 0.6	2.9 ± 0.4
$W(\to l\nu)$+ jets	452.3 ± 29.5	441.2 ± 20.5	28.9 ± 7.5	34.9 ± 5.9
Sum	538.9 ± 29.9	527.1 ± 20.7	31.8 ± 7.5	39.5 ± 5.9

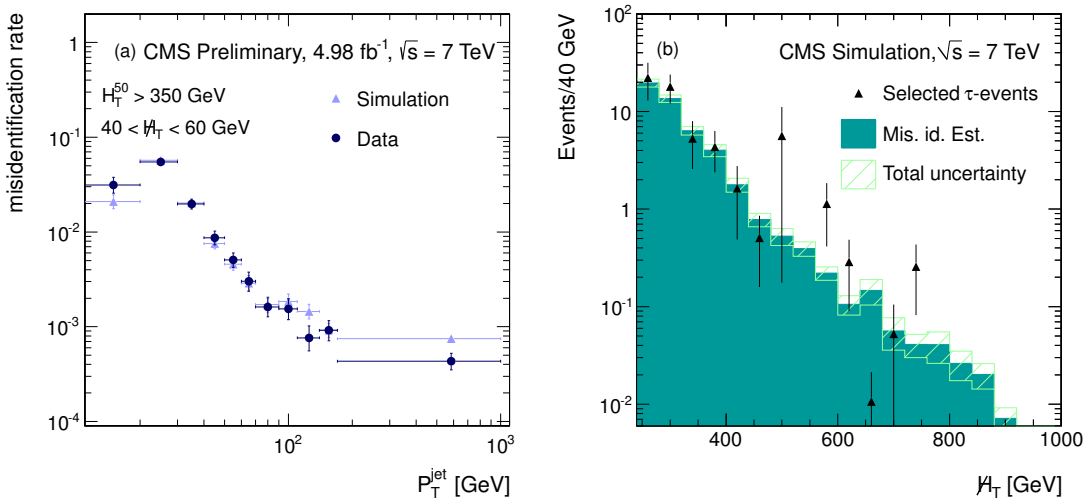

Figure 3: (a) Jet→ τ_h misidentification rates in simulation (colored markers) and data (dark markers) as a function of p_T^{jet} for events with $H_T^{50} > 350$ GeV and $40 < \not{H}_T < 60$ GeV. (b) $\not{H}_T$ distribution for the τ_h misidentification rate estimated in simulated events with $H_T^{50} > 350$ GeV, where the black dots represent the events which pass the baseline selection, the filled blue area shows the predicted events and the hashed area shows the total uncertainty on the prediction. These distributions correspond to the single τ_h final state.

The second largest contribution to the muon control sample is from $t\bar{t}$ events, where one W boson decays into a well identified muon while the other W boson decays hadronically into either a (unidentified) τ-lepton or into a light lepton which is subsequently lost. Any isolated muons produced through the decay of b quarks can also contribute to the single τ_h control sample. SM processes containing a Z boson or two W bosons can also contribute to the muon control sample if one of the two decay muons is lost. The true event yields of each process as determined by simulation are summarized in Table 1 for the baseline and full selection of the single τ_h final state.

For both the baseline and the full selection, the number of events with real τ_h's estimated from simulation are in good agreement with the number of selected events. The ε_τ that is used to calculate the predicted rate is measured in a sample of W + jets and is different from the ε_τ that would be measured in a sample of $t\bar{t}$ events. This leads to an overestimation of the $t\bar{t}$ contribution and a systematic uncertainty is assigned to account for this overestimation.

6.1.2 Estimate of the Fake-τ_h Background in the Single τ_h Final State

To estimate the background where a jet is misidentified as a τ_h, a jet dominated control sample is obtained by selecting events with $H_T^{50} > 350$ GeV and $40 < \not{H}_T < 60$ GeV. The control sample is selected with a prescaled H_T trigger with criteria that lead to a sample where $\sim 99\%$ of the events are multijet. Jets considered in the calculation of the misidentification rate satisfy the requirements of $p_T > 5$ GeV and $|\eta| < 2.5$. These jets are required to be within $\Delta R < 0.1$ from a τ_h candidate with $p_T > 15$ GeV and $|\eta| < 2.1$. The misidentification rates f_i for each jet i depend on η and p_T and are used to determine an overall weight which is applied to each event. The event weights are defined as:

$$f_{event}^{corr} = 1 - \prod_i (1 - f_i), \tag{3}$$

Table 2: The percentage of multijet events in the $\not{H}_T$ binned samples for different multijet dominated regions in the single τ_h final state is shown. This is used to test the background estimation method due to a misidentified τ_h. The ratio of selected events over predicted events is shown to be statistically compatible to one and the ratio is stable over the multijet dominated range of $60 < \not{H}_T < 100$ GeV (in the case of data, the ratio of selected/predicted $= 1.07 \pm 0.21$).

	$\not{H}_T$ [GeV]		
$H_T^{50} > 350$ GeV	60-80	80-100	> 250
QCD fraction	97%	93%	6%
selected/predicted (sim)	0.98 ± 0.06	0.96 ± 0.07	1.24 ± 0.28
selected/predicted (data)	1.01 ± 0.08	0.88 ± 0.13	-
$H_T^{50} > 600$ GeV			> 400
QCD fraction	96%	93%	17%
selected/predicted (sim)	0.94 ± 0.09	0.85 ± 0.09	2.43 ± 1.45
selected/predicted (data)	1.14 ± 0.26	0.97 ± 0.37	-

where $f_i = f_i(p_T^i, \eta^i)$ is the jet p_T and η dependent misidentification rate, $i = 1 \ldots n$, and n the number of jets. The measured misidentification rate is applied to data events in the region with $H_T^{50} > 350$ GeV and with $H_T^{50} > 600$ for two regions of $\not{H}_T$: $60(80) < \not{H}_T < 80(100)$ GeV. These are regions that are almost all multijet events. The results for data and simulation, as well as the fraction of multijet events are shown in Table 2. The ratio of selected events over predicted events is statistically compatible with one and stable over the range of $\not{H}_T$. Fig. 3b shows the $\not{H}_T$ distributions of predicted and selected events for simulated multijet events with $H_T^{50} > 350$ GeV. The two distributions agree over the whole range of $\not{H}_T$.

6.2 Estimate of Backgrounds in the $\tau_h\tau_h$ Final State

The estimate of the SM background contributions to the SR is based on observed events in control samples. The events in each CR are selected with most of the selection similar to those used in the main search but further enriched with events from the background process in question. Correction factors and/or selection efficiencies are measured in those CRs and used to extrapolate to the region where a signal might present itself. We use the observed jet multiplicity in each CR along with the measured jet $\rightarrow \tau_h$ misidentification rate to calculate the yield in the SR. The following equation is used to estimate each background contribution:

$$N^{\mathrm{SR}}_{Background} = N^{\mathrm{CR}}_{Background}[\alpha_{\tau\tau}\mathcal{P}(0) + \alpha_{\tau j}\mathcal{P}(1) + \alpha_{jj}\mathcal{P}(2)] \quad (4)$$

where $N^{SR}_{Background}$ is the predicted rate in the SR, $N^{CR}_{Background}$ is the observed number of events in the CR and α_{xy} is the correction factor for acceptance and efficiency for events in the CR with true physics objects "x" and "y". Here the physics object can be a τ_h or a quark/gluon jet. Since the dominant SM backgrounds contribute to the SR when jets are misidentified as τ_h, the general background estimation strategy outlined in Eq. 4 relies on the determination of the event probability, $\mathcal{P}(m)$, for at least "m" jets to be misidentified as τ_h. The calculation of the event probability $\mathcal{P}(m)$ contains three contributions: (i) the probability $P(N)$ for an event to contain N jets; (ii) the number of possible ways for exactly n jets to pass the τ_h identification criteria given N possible jets, $C(N,n) = \frac{N!}{n!(N-n)!}$, and (iii) the probability, f, for a single jet to be misidentified as a τ_h. In general, $\mathcal{P}(m)$ is given by:

$$\mathcal{P}(m) = \sum_{N=m}^{\infty} P(N) \sum_{n=m}^{N} C(N,n) f^n (1-f)^{N-n} \tag{5}$$

Eq. 5, if used in the case of the single τ_h final state, would be identical to Eq. 3. Eq. 4 is used to estimate the $t\bar{t}$, W + jets and Z + jets background contributions to the SR. The probability $P(N)$ for an event to contain N jets is determined from data using the jet multiplicity distribution in each CR. The jet$\rightarrow \tau_h$ misidentification rate f is measured for each background process by determining the fraction of jets in each CR which pass the τ_h identification criteria. Since the multijet contribution to the SR is expected to be very small and negligible based on simulation, a data-to-MC scale factor (SF) is used to correct the multijet prediction from simulation. In the sections that follow, the selection used to define high purity CRs are outlined and correction factors α_{xy} used in Eq. 4 are defined.

6.2.1 Estimate of $t\bar{t}$ Events in the $\tau_h\tau_h$ Final State

To estimate the $t\bar{t}$ contribution in the $\tau_h\tau_h$ SR, a control sample is obtained by requiring the presence of at least two jets identified as b jets using the track counting high efficiency (TCHEM) algorithm [23]. Because multijet, W + jets, $Z(\rightarrow \tau\bar{\tau})$ + jets and $Z(\rightarrow \nu\bar{\nu})$ + jets events are unlikely to contain two b jets, this requirement provides a sample in which $\sim 99\%$ of the events are $t\bar{t}$ events, according to simulation. Such a $t\bar{t}$ sample is obtained by removing the τ_h isolation requirement in addition to requiring at least two b jets in the event. Fig. 4a shows the τ_h p_{T} distribution in $t\bar{t}$ events for data and simulation. The fraction of events from the resulting $t\bar{t}$ control sample with $2\tau_h + 2b$, jet $+\tau_h + 2b$, and 2jets $+2b$ are denoted as $A_{\tau\tau}$, $A_{\tau j}$, and A_{jj} respectively. According to simulation, the fraction of events in the $t\bar{t}$ control sample which contains one real τ_h is $A_{\tau j} = 0.166 \pm 0.011$, while the fraction of events without a real τ_h is $A_{jj} = 0.834 \pm 0.025$. The real $\tau_h\tau_h$ contribution is negligible ($A_{\tau\tau} \sim 0$) according to simulation. Incomplete knowledge of the real $\tau_h\tau_h$ contribution is included as a source of systematic uncertainty on the $t\bar{t}$ prediction. Therefore, $\alpha_{\tau j}$ in Eq. 4 is given by $A_{\tau j}\frac{\varepsilon_\tau^{iso}}{P(2\ b\ \mathrm{jets})}$, where ε_τ^{iso} is the probability for a τ_h to pass the isolation requirement, while α_{jj} is given by $\frac{A_{jj}}{P(2\ b\ jets)}$. $P(2\ b\ jets)$ is the probability to identify ≥ 2 b jets and is measured by the b jet identification efficiency, ε_b [23]. The number of $t\bar{t}$ events in the SR is calculated as follows:

$$N_{t\bar{t}}^{\mathrm{SR}} = \frac{N_{t\bar{t}}^{\mathrm{CR}}}{P(2\ b\ jets)}[A_{\tau j}\varepsilon_\tau^{iso}\mathcal{P}(1) + A_{jj}\mathcal{P}(2)] \tag{6}$$

The probability for a jet in $t\bar{t}$ to be misidentified as a τ_h has a measured value of $f = 0.022 \pm 0.004$. Cross-checks are made to validate the use of the b jet identification efficiency as measured in [23] for this analysis. The estimated $t\bar{t}$ contribution in the SR is determined to be 2.03 ± 0.36.

6.2.2 Estimate of $Z(\rightarrow \nu\bar{\nu})$ + Jets Events in the $\tau_h\tau_h$ Final State

A highly pure control sample of $Z(\rightarrow \nu\bar{\nu})$ + jets events is difficult to obtain without significant modifications to the signal selection. Thus the contribution of $Z(\rightarrow \nu\bar{\nu})$ + jets to the signal sample is determined by selecting a sample of $Z(\rightarrow \mu\bar{\mu})$ + jets events and treating the muons as neutrinos in order to properly model the large $\not{H}_{\mathrm{T}}$ values associated with $Z(\rightarrow \nu\bar{\nu})$ + jets events. The sample is collected using a $\mu - \tau$ trigger. To select the control sample, jet selection criteria similar to the main search are used with the addition of requiring the presence of two

clean muons in the event. The control sample has a purity of $\sim 99\%$ as estimated in simulation. The $\not{H}_T$ distribution for events passing this criteria is shown in Fig. 4b. The $Z(\rightarrow \nu\bar{\nu})$ + jets background is estimated by interpreting the p_T of the pair of muons as $\not{H}_T$. In order to predict the $Z(\rightarrow \nu\bar{\nu})$ + jets rate in the search region, the $Z(\rightarrow \mu\bar{\mu})$ + jets sample is corrected for the branching ratios $R = B(Z \rightarrow \nu\bar{\nu})/B(Z \rightarrow \mu\bar{\mu})$, for trigger efficiencies, for the geometric acceptance, A_μ, as measured from simulation and from the reconstruction efficiency, ε_μ, as measured from data. Therefore, α_{jj} in Eq. 4 is given by $\frac{1}{A_\mu^2\varepsilon_\mu^2}\frac{B(Z\rightarrow\nu\bar{\nu})}{B(Z\rightarrow\mu\bar{\mu})}\frac{\varepsilon_{\not{H}_T}^{Trigger}}{\varepsilon_{\mu\tau}^{Trigger}}\varepsilon^{\not{H}_T}$. Since there is no prompt production of a real τ_h in the $Z(\rightarrow \mu\bar{\mu})$ + jets sample, $\alpha_{\tau j} = 0$ and $\alpha_{\tau\tau} = 0$. The $Z(\rightarrow \nu\bar{\nu})$ + jets contribution to the SR is calculated as follows:

$$N_{Z\rightarrow\nu\bar{\nu}+jets}^{SR} = \frac{N_{Z\rightarrow\mu\bar{\mu}+jets}^{CR}}{A_\mu^2\varepsilon_\mu^2}\frac{B(Z\rightarrow\nu\bar{\nu})}{B(Z\rightarrow\mu\bar{\mu})}\frac{\varepsilon_{\not{H}_T}^{Trigger}}{\varepsilon_{\mu\tau}^{Trigger}}\varepsilon^{\not{H}_T}\mathcal{P}(2) \quad (7)$$

$\varepsilon_{\not{H}_T}^{Trigger}$ is the $\not{H}_T$ trigger efficiency, and $\varepsilon_{\mu\tau}^{Trigger}$ the $\mu-\tau$ trigger efficiency. The efficiency for the $\not{H}_T > 250$ GeV signal selection ($\varepsilon^{\not{H}_T}$) is determined by calculating the fraction of the observed events in the CR which have $\not{H}_T > 250$ GeV. The muon identification efficiency ε_μ is measured using the standard tag-and-probe method. The probability for a jet to be misidentified as a τ_h has a measured value of $f = 0.0164 \pm 0.00193$. Therefore, the estimated $Z(\rightarrow \nu\bar{\nu})$ + jets contribution to the SR is determined to be 0.03 ± 0.02.

6.2.3 Estimate of $Z \rightarrow \tau\bar{\tau}$ + Jets Events in the $\tau_h\tau_h$ Final State

The contribution from $Z \rightarrow \tau\bar{\tau}$ events is determined using the same sample of $Z(\rightarrow \mu\bar{\mu})$ + jets events used to estimate $Z(\rightarrow \nu\bar{\nu})$ + jets, but the muons are treated as τ_h. The factors α_{xy} are more complicated for the estimation of $Z \rightarrow \tau\bar{\tau}$ since there are several ways in which $Z \rightarrow \tau\bar{\tau}$ can contribute to the SR: (i) both τ_h's pass the kinematic acceptance and identification criteria; (ii) both τ_h's pass the kinematic acceptance criteria, but only one passes the identification criteria; (iii) one τ_h fails the kinematic acceptance criteria, while the other τ_h passes both the kinematic acceptance and identification criteria; (iv) both τ_h's fail the kinematic acceptance criteria. Therefore, the $Z(\rightarrow \tau\bar{\tau})$ + jets contribution to the SR is calculated as follows:

$$N_{Z\rightarrow\tau\bar{\tau}}^{SR} = N_{Z\rightarrow\mu\bar{\mu}}^{CR} R\left[\frac{A_\tau^2\varepsilon_\tau^2}{A_\mu^2\varepsilon_\mu^2} + \frac{2A_\tau^2\varepsilon_\tau(1-\varepsilon_\tau)}{A_\mu^2\varepsilon_\mu^2}\mathcal{P}(1) + \frac{2A_\tau(1-A_\tau)\varepsilon_\tau}{A_\mu^2\varepsilon_\mu^2}\mathcal{P}(1) + \frac{(1-A_\tau)^2}{A_\mu^2\varepsilon_\mu^2}\mathcal{P}(2)\right] \quad (8)$$

where $R = \frac{B(Z\rightarrow\tau\bar{\tau})B^2(\tau\rightarrow\tau_h)}{B(Z\rightarrow\mu\bar{\mu})}\frac{\varepsilon_{\not{H}_T}^{Trig}}{\varepsilon_{\mu\tau}^{Trig}}\varepsilon^{\not{H}_T}$, A_τ is the τ_h acceptance efficiency and ε_τ is the τ_h identification efficiency in this control sample. The probability for a jet to be misidentified as a τ_h has a measured value of $f = 0.0164 \pm 0.00193$. Therefore, the estimated Z ($\rightarrow \tau\bar{\tau}$) + jets contribution to the SR is determined to be 0.21 ± 0.13.

6.2.4 Estimate of W + Jets Events in the $\tau_h\tau_h$ Final State

To select the W + jets control sample, the τ_h isolation criteria which discriminates a τ_h from other jets is dropped from the signal selection. However, the lack of the τ_h isolation requirement also increases the contribution from other backgrounds as most of the backgrounds arise due to jets being misidentified as τ_h. To minimize the contribution from $t\bar{t}$, events are required to have no jets identified as b jets. Although this selection minimizes the contamination from $t\bar{t}$ events to

$\sim$ 5%, the contributions from other backgrounds are not negligible. The control sample has a purity of $\sim$ 65%. Fig. 4c shows the $\not\!\!E_{\mathrm{T}}$ distribution for events in the W + jets dominated control sample. The non-negligible contributions of multijet events, $\mathrm{t\bar{t}}$, and $Z(\rightarrow \nu\bar{\nu})$ + jets processes are subtracted in order to determine the number of W + jets events in the CR. The predicted rates for multijet, $\mathrm{t\bar{t}}$ and $Z(\rightarrow \nu\bar{\nu})$ + jets events are determined by extrapolating from their corresponding CRs. The fraction of W + jets events from the resulting control sample with τ_h+jet and jet+jet are denoted as $A_{\tau j}$ and A_{jj} respectively. Since there is no prompt production of real $\tau_h\tau_h$ for W + jets, $\alpha_{\tau\tau} = 0$. According to simulation, the fraction of events in the control sample which contain one real τ_h is $A_{\tau j} = 0.149 \pm 0.016$, while the fraction of events without a real τ_h is $A_{jj} = 0.851 \pm 0.038$. Therefore, $\alpha_{\tau j}$ in Eq. 4 is given by $A_{\tau j}\frac{\varepsilon_\tau^{iso}}{P(0\ b\ jets)}$, where ε_τ^{iso} is the probability for a τ_h to pass the isolation requirement, while α_{jj} is given by $\frac{A_{jj}}{P(0\ b\ jets)}$. The probability for a W + jets event to have exactly zero light quark or gluon jets be misidentified as b jets is denoted as $P(0\ b\ \mathrm{jets})$. The contribution of W + jets events to the SR is then calculated as:

$$N_{W+jets}^{\mathrm{SR}} = \frac{N_{W+jets}^{After\ subtraction}}{P(0\ b\ jets)}[A_{\tau j}\varepsilon_\tau^{iso}\mathcal{P}(1) + A_{jj}\mathcal{P}(2)] \tag{9}$$

The jet$\rightarrow \tau_h$ misidentification rate is measured to be 0.019 ± 0.001. The jet$\rightarrow b$ misidentification rate, f_b [23], is used to calculate the probability $P(0\ b\ \mathrm{jets})$ The estimated W + jets contribution to the SR is determined to be 5.20 ± 0.63.

6.2.5 Estimate of Multijet Events in the $\tau_h\tau_h$ Final State

Multijet events contribute to the SR when mismeasurements of jet energies lead to large values of $\not\!\!H_{\mathrm{T}}$, and when jets are misidentified as τ_h's. By removing the τ_h isolation criteria and inverting the $|\Delta\phi(j_2, \not\!\!H_{\mathrm{T}})|$ requirement, a sample is obtained, where $\sim$ 99% of the events are multijet. Fig. 4d shows the expected and observed $\not\!\!H_{\mathrm{T}}$ distributions. A scale factor is obtained from this control sample and used to correct the signal prediction for multijet events in simulation. The estimated contribution to the SR from multijet events is measured to be 0.02 ± 0.02.

7 Systematic Uncertainties

Systematic uncertainties are taken into account for both the signal and background and are described separately. Both the signal and background are affected by the systematic uncertainty in the identification of the τ_h candidate. The systematic uncertainty for τ_h identification (7%) is obtained using a $Z \rightarrow \tau\bar{\tau}$ enhanced region and by correcting the cross section by that measured using $ee/\mu\mu$. This uncertainty is validated on a control sample of $Z \rightarrow \tau\bar{\tau}$ events which is selected using criteria similar to those used to select the search region and where the consistency between simulation and data is shown to be at the level of 7%. Further validation of the performance of τ_h identification in a SUSY-like environment is carried out by selecting a W($\rightarrow \tau\nu \rightarrow \tau_h\nu$'s) + jets control sample with large hadronic activity (H_{T}) and large transverse momentum imbalance ($\not\!\!H_{\mathrm{T}}$). The level of agreement between the predicted rate for W$\rightarrow \tau\nu \rightarrow \tau_h\nu$ and the observed number of events is within 7% and is determined as a function of H_{T} and $\not\!\!H_{\mathrm{T}}$.

7.1 Systematic Uncertainties on Backgrounds

The dominant source of systematic uncertainties on the background predictions are due to uncertainties in the correction factors, statistical uncertainties on the number of events in the CRs, uncertainties in the measured jet$\rightarrow \tau_h$ misidentification rates, and the level of agreement between predicted rates and observed number of events in the CRs.

The contributions to the uncertainties in the correction factors are different for each background in question. However, in general, the dominant effect is due to the uncertainty in the τ_h identification efficiency. In the $\tau_h\tau_h$ final state, jet energy correction (JEC) uncertainties [24] and τ_h energy scale (TES) [25] systematics are used to quantify how the changes in $H_T/\not{H}_T$ and jet kinematics result in systematic shifts in the correction factors. The systematic uncertainty on the correction factors due to JEC and TES is at most $\sim 3\%$ for all backgrounds. There are smaller contributions to the uncertanties in the correction factors due to muon reconstruction and isolation efficiency ($< 1\%$), the uncertainty in the branching fractions ($\ll 1\%$), and the trigger inefficiency due to muon smearing (1%).

The systematic uncertainties on the measured jet$\rightarrow \tau_h$ misidentification rates are dominated by the size of the jet sample used to measure these rates and range from 2% in the single τ_h final state to $5.6-10\%$ in the $\tau_h\tau_h$ final state. The level of agreement between the predicted rates and observed number of events in each CR is used to assign an additional systematic uncertainty and ranges from 2% for the single τ_h final state to 3% for the $\tau_h\tau_h$ final state. Finally, any systematic uncertainty arising from statistical uncertainties on the number of events in the CRs ranges from $2-5\%$ in the $\tau_h\tau_h$ final state to $3-10\%$ in the single τ_h final state.

7.2 Systematic Uncertainties on Signal

The main sources of systematics in the SR are due to trigger efficiencies, identification efficiencies, energy and momentum scale, luminosity measurement, parton distribution functions, and initial and final state radiation. The uncertainty in the luminosity measurement is 2.2% [26, 27]. Systematic uncertainties on the $\not{H}_T$ triggers (2.5%) are measured using a sample where $\sim 99\%$ of the events are $t\bar{t}$ which have a topology similar to the SR. The systematic uncertainties due to the τ_h and jet energy scale (3.0%) affect our knowledge of the signal acceptance by 2.3%. The uncertainty on the $\not{E}_T$ scale depends on the uncertainty of the jet energy scale ($2-5\%$ depending on η and p_T of the jet) and on the unclustered energy scale (10%). Unclustered energy is defined as the energy found "outside" any reconstructed leptons and jets with $p_T > 10$ GeV. The unclustered energy scale uncertainty has a negligible systematic effect on the signal acceptance. The systematic effect due to imprecise knowledge of the parton distribution functions (11%) is determined by comparing CTEQ6.6L[28], MSTW 2008 NLO [29] and NNPDF2.1 [30] PDF with the default PDF. The systematic effect due to imprecise modeling of initial and final state radiation is determined by re-weighting events to account for effects such as the missing α terms in the soft-collinear approach [31] and missing NLO terms in the parton shower approach [32]. The systematic effect due to the imprecise modeling of the initial and final state radiation is negligible. The systematic effects due to pile up are also negligible.

8 Results

This analysis has been performed with CMS data corresponding to a luminosity of 4.98 fb^{-1}. For the single τ_h final state, the number of background events containing a real τ_h, as well as the number of background events containing a misidentified τ_h is estimated with data. The results for the baseline and the full selection are listed in Table 3. Fig. 5 shows the H_T^{50} and $\not{H}_T$

Table 3: Number of observed data events and estimated background rates in the single τ_h final state.

Process	Baseline	Signal Region
Fake$-\tau_h$	$67 \pm 2_{stat} \pm 19_{syst}$	$3.4 \pm 0.4_{stat} \pm 1.0_{syst}$
Real$-\tau_h$	$367 \pm 10_{stat} \pm 27_{syst}$	$25.9 \pm 2.5_{stat} \pm 2.3_{syst}$
Estimated $\sum SM$	$434 \pm 10_{stat} \pm 33_{syst}$	$29.3 \pm 2.6_{stat} \pm 2.5_{syst}$
Observed $Data$	444	28

distributions of data and the different background predictions. The observed number of events in data is in agreement with the data-driven SM predictions. No deviations from SM physics have been observed.

The largest sources of background for the $\tau_h\tau_h$ final state are from $\bar{t}t$ and W + jets events. A counting experiment is performed and the data-driven predictions are compared to the observed number of events. Table 4 lists the data-driven background predictions and observed number of events in the SR. Fig. 6 shows the H_T^{30} as well as the $M_{eff}(= \not{H}_T + H_T^{30})$ distributions in the SR. The background distributions in Fig. 6 are taken from simulation and normalized to the data-driven predictions over the full spectrum. The estimated number of events due to the SM background processes are in agreement with the number of observed events in the SR. No deviation from SM physics has been observed.

Table 4: Number of observed data events and estimated background rates in the $\tau_h\tau_h$ final state.

Process	Signal Region
multijet events	$0.02 \pm 0.02_{stat} \pm 0.17_{syst}$
W+jets	$5.20 \pm 0.63_{stat} \pm 0.62_{syst}$
$\bar{t}t$	$2.03 \pm 0.36_{stat} \pm 0.34_{syst}$
$Z(\rightarrow \tau\bar{\tau})+$ jets	$0.21 \pm 0.13_{stat} \pm 0.17_{syst}$
$Z(\rightarrow \nu\bar{\nu})+$ jets	$0.03 \pm 0.02_{stat} \pm 0.50_{syst}$
Estimated $\sum SM$	$7.49 \pm 0.74_{stat} \pm 0.90_{syst}$
Observed $Data$	9
$[m_0, m_{1/2}] = [280, 320]$	$7.1 \pm 1.2_{stat}$

9 Limits on New Physics

The observed number of events in the single τ_h and $\tau_h\tau_h$ final states do not reveal any evidence of physics beyond the standard model. Therefore, exclusion limits are set using the CL_S [33] criterion in the context of cMSSM and SMS. The excluded regions of cMSSM parameter space at fixed $\tan\beta = 40$, $A_0 = 500$ GeV, $\mu > 0$ and $M_{top} = 173.2$ GeV are shown for the single τ_h and $\tau_h\tau_h$ final states in Fig. 7a and Fig. 7b respectively [34]. The limits are set using a cut and count method. Systematics are treated as nuissance parameters and marginalized. Bands on the expected limits are determined by running pseudoexperiments using a background only hypothesis. The bands on the observed limits are driven by the theoretical uncertainties on the signal cross-sections. Scale variations of a factor of 2 as well as the PDF effects on the theoretical cross-sections are considered [35]. Using the limits set by the single τ_h analysis, a gaugino mass, $m_{1/2}$, of < 495 GeV is excluded at 95% CL for scalar masses, m_0, < 400 GeV. For the $\tau_h\tau_h$ analysis, $m_{1/2} < 495$ GeV is excluded at 95% CL for $m_0 = 400$ GeV. Since the gluino mass is mostly determined by $m_{1/2}$, a gluino with mass < 1.15 TeV is excluded at 95% CL.

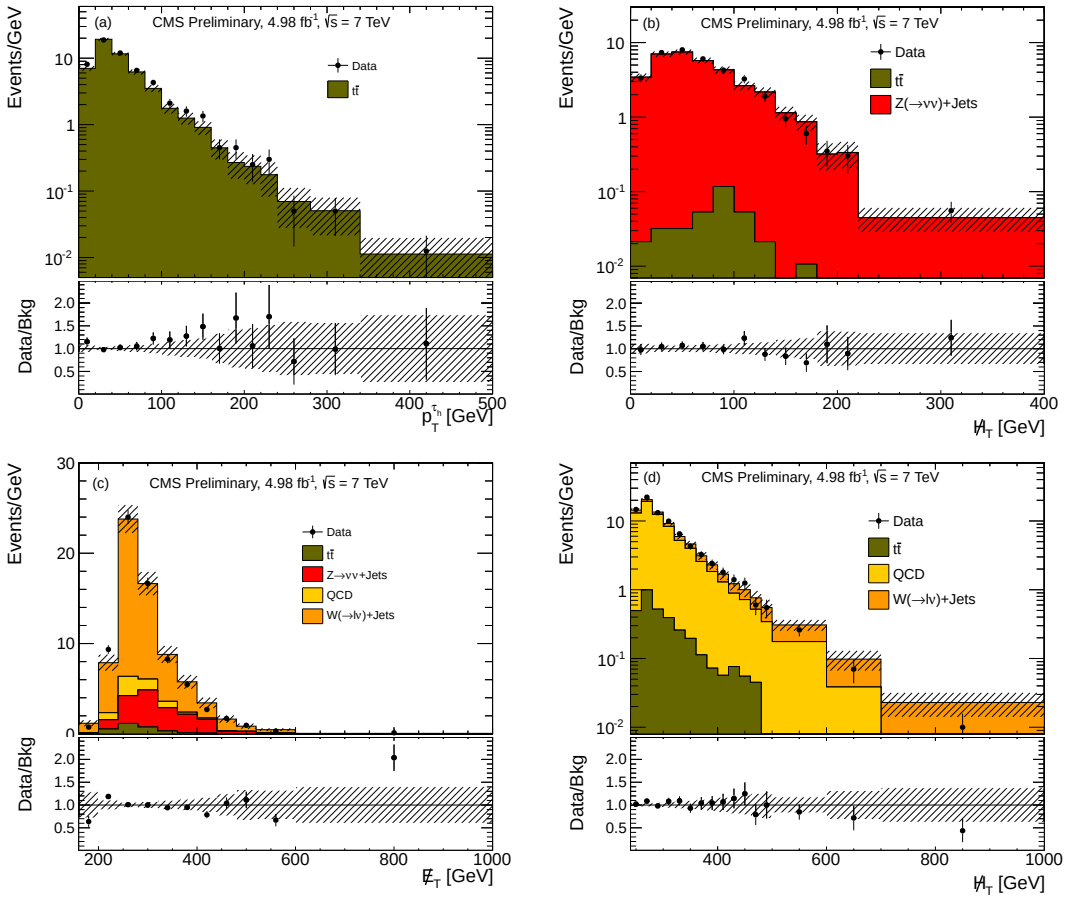

Figure 4: Plots comparing data to the results of MC simulation for the $\tau_h\tau_h$ final state, which include (a) p_T distribution of the τ_h candidate in the $t\bar{t}$ CR, (b) $\not{H}_T$ distribution in the $Z(\rightarrow \mu\mu)$ + jets CR which is used to estimate the number of $Z(\rightarrow \nu\nu)$ + jets events, (c) $\not{E}_T$ distribution in the W + jets CR, and (d) SM background enhanced sample depicting the effectiveness of $|\Delta\phi(j_2, \not{H}_T)| < 0.1$ in selecting a sample where $\sim 99\%$ of the events are multijet.

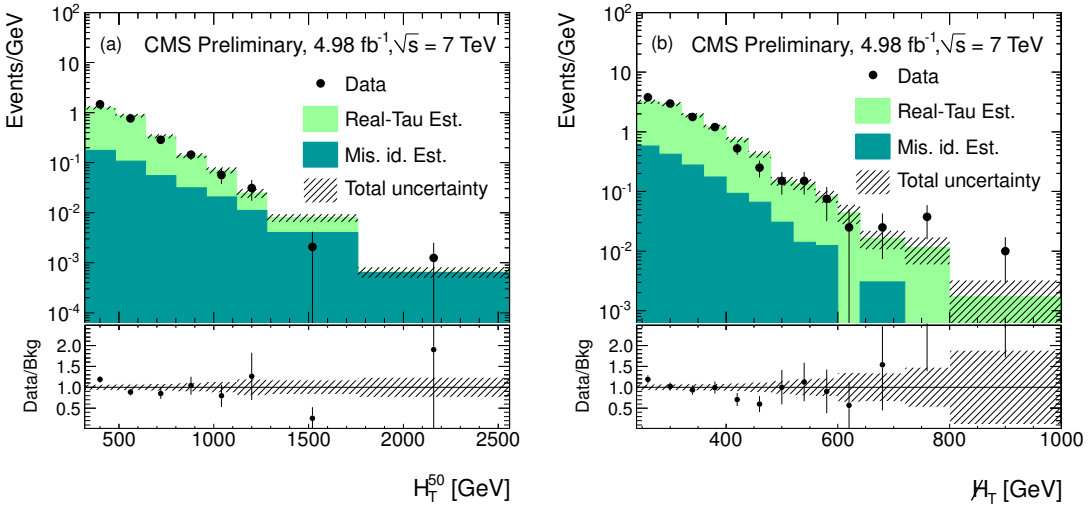

Figure 5: (a) Distributions of H_T^{50} and (b) $\not{H}_T$ for the single τ_h final state. The black dots represent the events in data which pass the baseline selection while the filled green (light) and filled blue (dark) areas shows the predicted backgrounds due to events containing a real τ_h and a misidentified τ_h respectively. The hashed area shows the total uncertainty on the prediction.

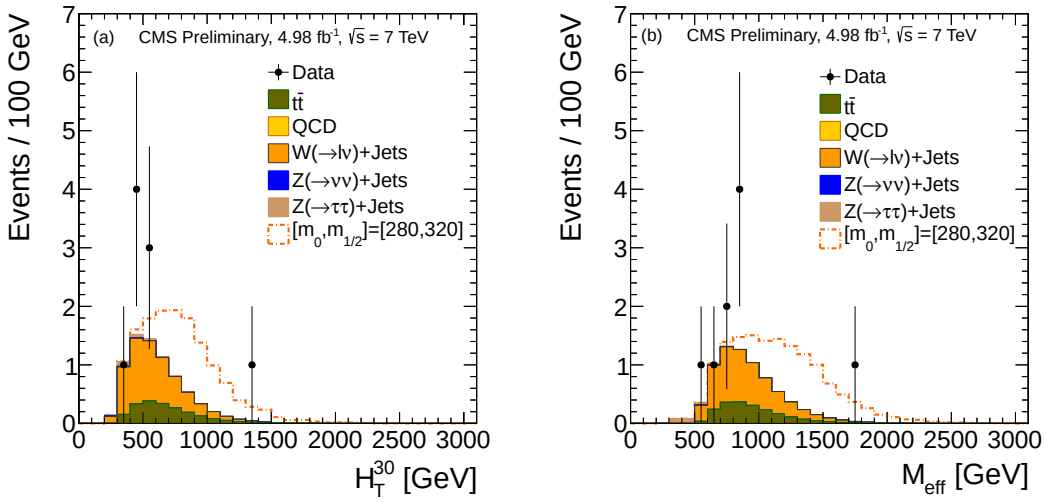

Figure 6: (a) Distributions of H_T^{30} and (b) $M_{eff} = (\not{H}_T + H_T^{30})$ in the SR for the $\tau_h\tau_h$ final state. The background distributions are taken from MC events which are normalized to the data-driven predictions over the full region. The shapes obtained from MC simulation are used for illustrative purposes.

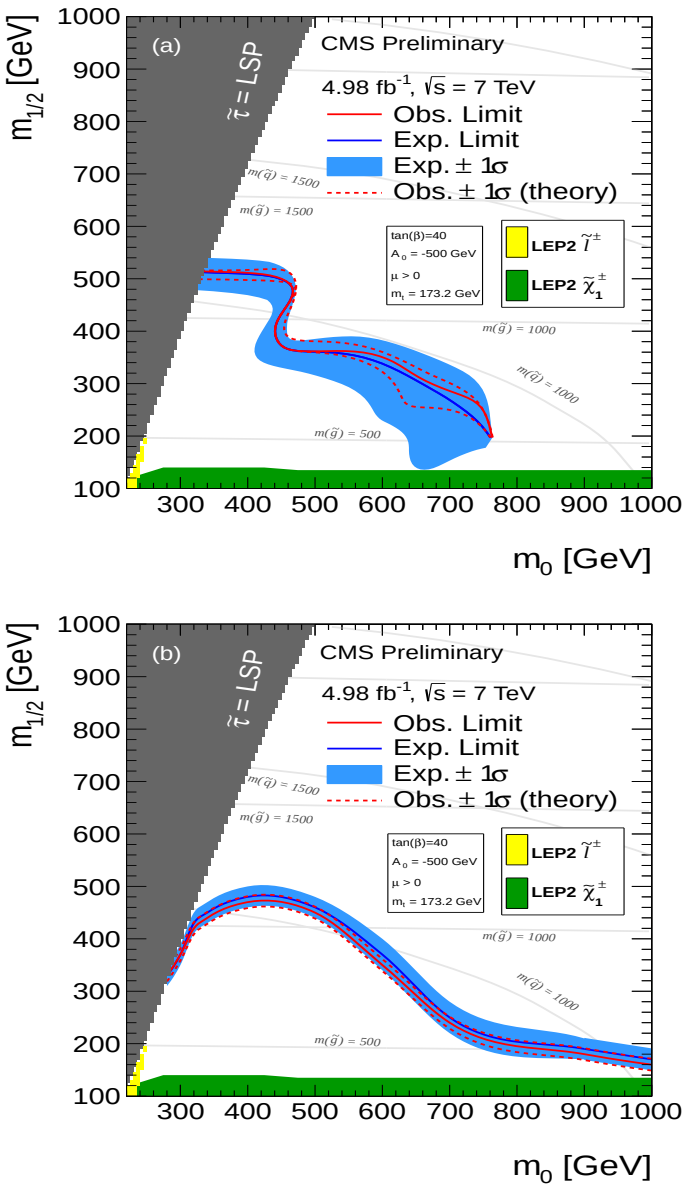

Figure 7: (a) Exclusion limits in the cMSSM plane at $\tan\beta = 40$ for the single τ_h final state. The observed and expected limits are shown by the solid red and blue lines respectively. The blue band represents the expected uncertainties while the red dotted lines represent the theoretical uncertainties for events passing the full selection. (b) Exclusion limit in the cMSSM plane at $\tan\beta = 40$ for the $\tau_h\tau_h$ final state. The solid red line denotes the experimental limit while the dotted red lines represent the uncertainty on the experimental limit due to scale variations by a factor of 2, and PDF effects on the theoretical cross sections. The blue band represents the expected uncertainties.

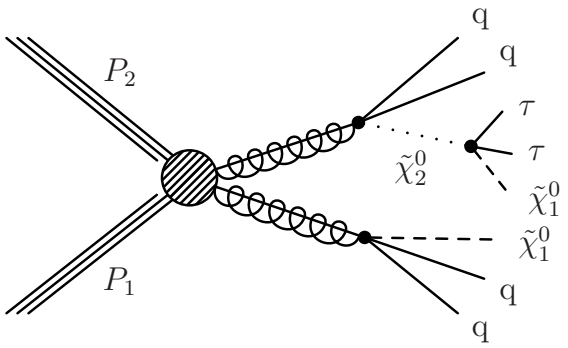

Figure 8: Feynman diagram for the T3tauh SMS model.

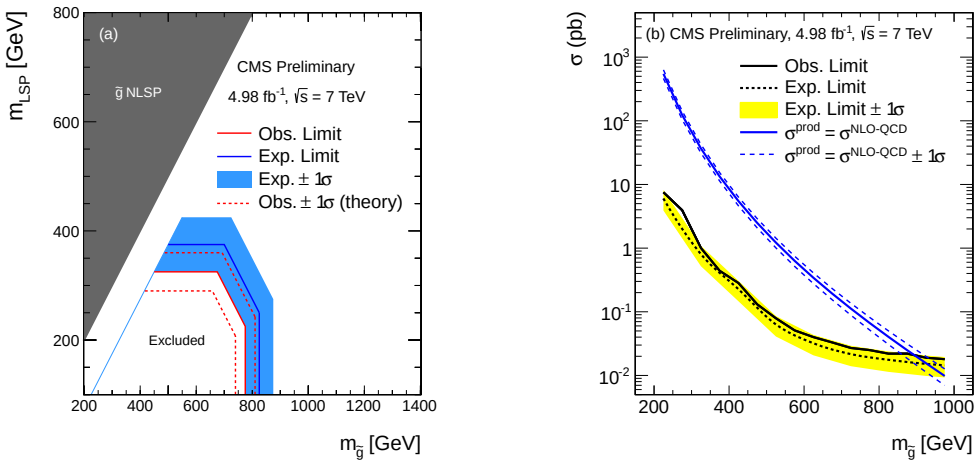

Figure 9: SMS exclusion limits are shown for the $\tau_h\tau_h$ final state. (a) 95% CL cross section upper limits for the T3tauh model where the solid red line represents the limits on the mass of the gluino and the LSP. (b) 95% CL cross section upper limits as a function of gluino mass in the GMSB scenario.

The results for the $\tau_h\tau_h$ final states are also interpreted in the context of SMS [11]. The T3tauh scenario is studied where gluinos are produced in pairs and subsequently decay to τ-lepton pairs and an LSP via a neutralino ($\tilde{g} \rightarrow q\bar{q}\tilde{\chi}_2^0$; $\tilde{\chi}_2^0 \rightarrow \tau + \bar{\tau}$+LSP). The Feynman diagram for the T3tauh model is given in Fig. 8. A gluino mass of < 740 GeV is excluded at 95% CL for LSP masses up to 290 GeV. Fig. 9a shows the 95% CL cross section upper limits obtained for T3tauh. The limits on the mass of the gluino and LSP are shown with a solid black line.

In the simplified Gauge Mediated Symmetry Breaking (GMSB) scenario, the $\tilde{\tau}$ is the NLSP and decays to a τ-lepton and a gravitino, $\tilde{G}$, with a mass of the order of $\sim$ keV [36–38] ($\tilde{\chi}_2^0 \rightarrow \tau\tilde{\tau} \rightarrow \tau\tau\tilde{G}$). The topology for this simplified GMSB scenario is similar to that of T3tauh. Therefore, the results are also interpreted in the simplified GMSB scenario using the T3tauh scenario. It is assumed that both gluinos decay to τ-lepton pairs with a branching fraction of 100%. The signal acceptance is corrected to account for the correct final state containing up to four τ-leptons. A gluino with mass < 860 GeV is excluded at 95% CL. Fig. 9b shows the exclusion limits for the simplified GMSB scenario as a function of the gluino mass.

Since the topologies we have considered in this paper are characterized by two τ-leptons in the final state, SMS limits for the single τ_h final state have not been studied.

10 Summary

A search for physics beyond the standard model with one or more hadronically decaying τ-leptons, highly energetic jets, and large momentum imbalance in the final state is presented. The data sample corresponds to an integrated luminosity of 4.98 ± 0.11 fb^{-1} of pp collisions at $\sqrt{s} = 7$ TeV collected with the CMS detector. The final number of events selected in data being consistent with the predictions for SM processes, no evidence of suspersymmetry has been observed. Upper limits on the signal cross section are set in the context of a simplified GMSB scenario. Within the cMSSM model, a gaugino mass, $m_{1/2}$, of < 495 GeV is excluded at 95% CL for scalar masses, m_0, < 400 GeV. This corresponds to a limit in the mass of the gluino of < 1.15 TeV within this constrained model. In the $\tau_h\tau_h$ final state, a gluino with mass < 740 GeV is excluded for the T3tauh simplified model while a gluino with mass < 860 GeV is excluded for the simplified GMSB scenario at 95% CL.

Acknowledgements

We congratulate our colleagues in the CERN accelerator departments for the excellent performance of the LHC machine. We thank the technical and administrative staff at CERN and other CMS institutes. This work was supported by the Austrian Federal Ministry of Science and Research; the Belgium Fonds de la Recherche Scientifique, and Fonds voor Wetenschappelijk Onderzoek; the Brazilian Funding Agencies (CNPq, CAPES, FAPERJ, and FAPESP); the Bulgarian Ministry of Education and Science; CERN; the Chinese Academy of Sciences, Ministry of Science and Technology, and National Natural Science Foundation of China; the Colombian Funding Agency (COLCIENCIAS); the Croatian Ministry of Science, Education and Sport; the Research Promotion Foundation, Cyprus; the Ministry of Education and Research, Recurrent financing contract SF0690030s09 and European Regional Development Fund, Estonia; the Academy of Finland, Finnish Ministry of Education and Culture, and Helsinki Institute of Physics; the Institut National de Physique Nucléaire et de Physique des Particules / CNRS, and Commissariat à l'Énergie Atomique et aux Énergies Alternatives / CEA, France; the Bundesministerium für Bildung und Forschung, Deutsche Forschungsgemeinschaft, and Helmholtz-Gemeinschaft Deutscher Forschungszentren, Germany; the General Secretariat for Research and Technology, Greece; the National Scientific Research Foundation, and National Office for Research and Technology, Hungary; the Department of Atomic Energy and the Department of Science and Technology, India; the Institute for Studies in Theoretical Physics and Mathematics, Iran; the Science Foundation, Ireland; the Istituto Nazionale di Fisica Nucleare, Italy; the Korean Ministry of Education, Science and Technology and the World Class University program of NRF, Korea; the Lithuanian Academy of Sciences; the Mexican Funding Agencies (CINVESTAV, CONACYT, SEP, and UASLP-FAI); the Ministry of Science and Innovation, New Zealand; the Pakistan Atomic Energy Commission; the Ministry of Science and Higher Education and the National Science Centre, Poland; the Fundação para a Ciência e a Tecnologia, Portugal; JINR (Armenia, Belarus, Georgia, Ukraine, Uzbekistan); the Ministry of Education and Science of the Russian Federation, the Federal Agency of Atomic Energy of the Russian Federation, Russian Academy of Sciences, and the Russian Foundation for Basic Research; the Ministry of Science and Technological Development of Serbia; the Secretaría de Estado de Investigación, Desarrollo e Innovación and Programa Consolider-Ingenio 2010, Spain; the Swiss Funding Agencies (ETH Board, ETH Zurich, PSI, SNF, UniZH, Canton Zurich, and SER); the National Science Council, Taipei; the Scientific and Technical Research Council of Turkey, and Turkish Atomic Energy Authority; the Science and Technology Facilities Council, UK; the US Department of Energy, and the US National Science Foundation.

Individuals have received support from the Marie-Curie programme and the European Research Council (European Union); the Leventis Foundation; the A. P. Sloan Foundation; the Alexander von Humboldt Foundation; the Belgian Federal Science Policy Office; the Fonds pour la Formation à la Recherche dans l'Industrie et dans l'Agriculture (FRIA-Belgium); the Agentschap voor Innovatie door Wetenschap en Technologie (IWT-Belgium); the Council of Science and Industrial Research, India; the Compagnia di San Paolo (Torino); and the HOMING PLUS programme of Foundation for Polish Science, cofinanced from European Union, Regional Development Fund.

References

[1] J. Gunion, H. Haber, G. Kane et al., "The Higgs Hunter's Guide", *Westview Press* (2000) ISBN 9780738203058.

[2] S. P. Martin, "A Supersymmetry primer", arXiv:hep-ph/9709356.

[3] D. Spergel et al., "First Year Wilkinson Microwave Anisotropy Probe (WMAP) Observations: Determination of Cosmological Parameters", *Astrophys. J. Suppl. Ser. 148* (2003) 175.

[4] G. Bertone, D. Hooper, and J. Silk, "Particle dark matter: Evidence, candidates and constraints", *Phys. Rept. 405* (2005) 279, doi:10.1016/j.physrep.2004.08.031, arXiv:hep-ph/0404175.

[5] H. Baer, "TASI 2008 lectures on Collider Signals. II. Missing E_T signatures and the dark matter connection", arXiv:0901.4732.

[6] K. Griest and D. Seckel, "Three exceptions in the calculation of relic abundances", *Phys. Rev. D 43* (1991) 3191.

[7] R. Arnowitt et al., "Determining the Dark Matter Relic Density in the Minimal Supergravity Stau-Neutralino Coannihilation Region at the Large Hadron Collider", *Phys. Rev. Lett. 100* (2008) 231802.

[8] G. L. Kane et al., "Study of constrained minimal supersymmetry", *Phys. Rev. D 49* (1994) 6173, doi:10.1103/PhysRevD.49.6173.

[9] A. H. Chamseddine, R. L. Arnowitt, and P. Nath, "Locally Supersymmetric Grand Unification", *Phys. Rev. Lett. 49* (1982) 970, doi:10.1103/PhysRevLett.49.970.

[10] J. Alwall, P. Schuster, and N. Toro, "Simplified Models for a First Characterization of New Physics at the LHC", *Phys. Rev. D79* (2009) 075020, arXiv:0810.3921.

[11] D. Alves et al., "Simplified Models for LHC New Physics Searches", arXiv:1105.2838.

[12] CMS Collaboration, "The CMS experiment at the CERN LHC", *J. Instrum. 0803* S08004.

[13] M. Cacciari, G. P. Salam, and G. Soyez, "The Anti-k(t) jet clustering algorithm", *JHEP 0804* (2008) 063, doi:10.1088/1126-6708/2008/04/063, arXiv:0802.1189.

[14] CMS Collaboration, "Commissioning of the Particle-Flow Reconstruction in Minimum-Bias and Jet Events from pp Collisions at 7 TeV", *CMS Physics Analysis Summary CMS-PAS-PFT-10-002* (2010).

[15] CMS Collaboration, "Performance of muon identification in pp collisions at $\sqrt{s} = 7$ TeV", *CMS Physics Analysis Summary CMS-PAS-MUO-10-002* (2010).

[16] CMS Collaboration, "Electron reconstructiona and identification at $\sqrt{s} = 7$ TeV", *CMS Physics Analysis Summary CMS-PAS-EGM-10-004* (2010).

[17] CMS Collaboration, "Particle Flow Event Reconstruction in CMS and Performance for Jets, Taus, and $\not{E}_{\mathrm{T}}$", *CMS Physics Analysis Summary CMS-PAS-PFT-09-001* (2009).

[18] CMS Collaboration, "Performance of tau reconstruction algorithms in 2010 data collected with CMS", *CMS Physics Analysis Summary CMS-PAS-TAU-11-001* (2011).

[19] T. Sjostrand, S. Mrenna, and P. Z. Skands, "PYTHIA 6.4 Physics and Manual", *JHEP 0605* (2006) 026, doi:10.1088/1126-6708/2006/05/026, arXiv:hep-ph/0603175.

[20] J. Alwall, "MadGraph/MadEvent v4: The New Web Generation", *JHEP 2007* (2007) 028, doi:10.1088/1126-6708/2007/09/028.

[21] Z. Was et al., "TAUOLA the library for tau lepton decay", *arXiv:hep-ph/0011305v1* (2000).

[22] GEANT4 Collaboration, "GEANT4: A Simulation toolkit", *Nucl.Instrum.Meth. A506* (2003) 250, doi:10.1016/S0168-9002(03)01368-8.

[23] CMS Collaboration, "b-jet Identification in the CMS Experiment", *CMS Physics Analysis Summary CMS-PAS-BTV-11-004* (2011).

[24] CMS Collaboration, "Determination of jet energy calibration and transverse momentum resolution in CMS", *J. Instrum. 6* (2011) P11002.

[25] CMS Collaboration, "Performance of τ-lepton reconstruction and identification in CMS", *J. Instrum. 7* (2012) P01001, doi:10.1088/1748-0221/7/01/P01001.

[26] CMS Collaboration, "Measurement of CMS Luminosity", *CMS Physics Analysis Summary CMS-PAS-EWK-10-002* (2010).

[27] CMS Collaboration, "Absolute Calibration of the Luminosity Measurement at CMS: Winter 2012 Update", *CMS Physics Analysis Summary CMS-PAS-SMP-12-008* (2012).

[28] P. M. Nadolsky, H.-L. Lai, Q.-H. Cao et al., "Implications of CTEQ global analysis for collider observables", *Phys. Rev. D78* (2008) 013004, doi:10.1103/PhysRevD.78.013004.

[29] A. Martin, W. Stirling, R. Thorne et al., "Parton distributions for the LHC", *Eur.Phys.J. C63* (2009) 189–285, doi:10.1140/epjc/s10052-009-1072-5.

[30] R. Ball, L. D. Debbio, A. Guffanti et al., "A first unbiased global NLO determination of parton distributions and their uncertainties", arXiv:1002.4407.

[31] G. Nanava et al., "How to use SANC to improve the PHOTOS Monte Carlo simulation of bremsstrahlung in leptonic W-Boson decays", *hep-ph/0303260* (2003).

[32] G. Miu et al., "W Production in an Improved Parton-Shower Approach", *hep-ph/9812455* (1998).

[33] P. D. G. Collaboration, "Review of Particle Physics", *J. Phys. G 37* (2010).

[34] M. Matchev and R. Remington, "Updated templates for the interpretation of LHC results on supersymmetry in the context of mSUGRA", arXiv:1202.6580v2.

[35] M. Krmer, A. Kulesza, M. Mangano et al., "Supersymmetry production cross sections in pp collisions at sqrts = 7 TeV", arXiv:1206.2892.

[36] M. Dine and W. Fishler *Phys. Lett. B 110* (1982) 227.

[37] C. R. Nappi and B. A. Ovrut *Phys. Lett. B 113* (1982) 175.

[38] L. Alvarez-Gaume, M. Claudson, and M. B. Wise *Nucl. Phys. B 207* (1982) 96.